PIER C

(Received 13 March 2024, Accepted 7 May 2024, Scheduled 15 May 2024)

Machine Learning-Based Optimization of Hexagon-Shaped Fractal Antenna for Ultra-Wideband Communications

Sai Sampreeth Indharapu[1, 2, *], Anthony N. Caruso[1, 2], Travis D. Fields[1, 2], and Kalyan C. Durbhakula[2]

[1] *School of Science and Engineering, University of Missouri-Kansas City, Kansas City, MO 64110, USA*
[2] *Missouri Institute for Defense and Energy, University of Missouri-Kansas City, Kansas City, MO 64110, USA*

ABSTRACT: In the wireless communication industry, achieving gigabit-per-second data rates with low-profile, ultra-wideband (UWB) microstrip patch antennae poses a significant challenge. Conventional optimization algorithms, though effective, are often computationally expensive, particularly for complex antenna geometries with high degrees of freedom. There is an imperative need for new methodologies to address this challenge and revolutionize the antenna optimization process. Successful and timely development of antennas relies on the efficiency and computational speed of optimization algorithms, full-wave electromagnetic solvers, and the intuition of radio frequency engineers. To mitigate the dependence on complex and time-consuming processes, we propose an efficient machine learning (ML)-based antenna optimization methodology that minimizes optimization time by more than 90%. This paper aims to apply and study the performance of two specific ML models, the radial basis function (RBF), and the least squared regression (LSR) models, in the bandwidth optimization without increasing the aperture area of a hexagon-shaped fractal antenna. The hexagon-shaped fractal antenna was chosen for its UWB characteristics, low profile, and high degrees of freedom (10 adjustable parameters). The reflection coefficient response of a hexagon-shaped fractal antenna is predicted by the trained RBF and LSR models and further optimized by the genetic algorithm (GA). The proposed approach stands out among other notable works in this research domain, especially for UWB applications, by prioritizing the optimization of the mean of the reflection coefficient across the entire frequency range instead of solely targeting individual frequency points. The GA-based optimization using trained ML models has increased the bandwidth by 21.3% and reduced the computational time by 90% compared to conventional optimization without increasing the physical or electrical size of the antenna. Simulation and measurement results concurred with a maximum difference of 5%, demonstrating the efficacy of the ML approach for antenna optimization.

1. INTRODUCTION

Ultra-wideband (UWB) microstrip (patch) antennas are seeing a 100x increase in demand in wireless communication systems, including satellite and radio applications [1], ground penetrating radars [2], bio-radars [3], GSM & LTE communications [4], microwave imaging [5], and phased-array radars [6]. UWB patch antennas are particularly popular for their low profile, medium to high gain (4–10 dBi), and ease of fabrication. The popularity of patch antennas is reflected in a 700% increase in publications over the last decade, highlighting the need for rapid and accurate optimization. However, most UWB patch antennas have complicated structures or geometries, with many adjustable parameters, making it tedious to perform a parametric study using commercially available full-wave electromagnetic (EM) solvers. The time required for a single full-wave EM simulation can vary from a few minutes to days, depending on the antenna's complexity [7]. Traditional optimization techniques [8–12] have been at the forefront for a long time in finding the optimum design values, but the trade-off is computational complexity, as they call the EM solvers iteratively, i.e., anywhere from a few 100 to 10000 iterations or epochs [7]. Optimization techniques typically employ a fitness function to determine optimal values. This objective function solves a specific problem, such as using EM solvers to calculate full-wave solutions for antenna design. However, the process of iteratively interacting with EM solvers within optimization algorithms to find the best values can be computationally demanding and time-consuming. Machine learning (ML) models, known for their adaptability, offer a potential solution to this problem. In this article, we present a detailed study and comparison of conventional optimization and ML-assisted optimization. Although ML models have been extensively used in fields such as biometrics [13–15], healthcare [16–18], and finance [19, 20], their application in electromagnetics and antenna design optimization is relatively new [21]. Previous studies have utilized various ML models to optimize antenna designs, as summarized in [22]. For instance, [23] replaced EM solvers with trained ML models such as Lasso, artificial neural network (ANN), and k-nearest neighbor (kNN) models, with a training data size of 450. In [24], an ANN was applied with a training data size of 110. These studies have demonstrated promising results in reduced time. However, the total computational time (C_t) required to generate training data depends on the complexity of the antenna design and the time required for EM software to simulate a single sample (C_s), as shown in

* Corresponding author: Sai Sampreeth Indharapu (sinf5@umsystem.edu).

Equation (1).

$$C_t = \sum_{i=1}^{n} (C_s) \tag{1}$$

Generating extensive training data is impractical and inefficient for all antenna designs, particularly those with complex designs and UWB characteristics. This paper presents a novel approach that eliminates the need for extensive training data by (1) performing a tradespace analysis of the selected antenna design to identify the most significant design features, (2) generating training data by varying values within the range of interest of the identified design features, and (3) training the selected ML models and using them as fitness functions for the optimization algorithm. This approach minimizes the need for extensive computational resources, enabling optimization algorithms to explore a broad range of designs and enhancing antenna design optimization objectives.

The optimal values obtained through the proposed methodology are compared and validated using the results obtained from both simulation and prototyped designs, as outlined in Section 3. The complete process was carried out using optimization software Altair HyperStudy [25] and numerical EM simulation from Altair FEKO[2].

2. ANTENNA DESIGN AND ANALYSIS

UWB antennas include various designs, such as planar inverted-f antenna (PIFA), biconical antenna, and logperiodic dipole array. Nevertheless, it is important to note that the proposed methodology can be applied to any antenna, regardless of the frequency range of operation, number of design variables, antenna size, or antenna design optimization objective. The decision to select the hexagon-shaped fractal antenna design over these renowned counterparts was motivated by its capacity for multi-band operations and space-filling properties. Additionally, a co-planar waveguide (CPW) was employed because of its advantages, such as broad bandwidth, ease of fabrication, and reduced losses due to its planar structure and ease of tuning.

Our study focuses on a single CPW monopole antenna integrated with fractal elements, drawing inspiration from [26]. The antenna configuration comprises a hexagonal patch featuring fractal elements at each corner, enhancing its performance characteristics. Fabricated on an FR-4 substrate with a thickness of 1.5 mm, a relative permittivity (ε_r) of 4.4, and a loss tangent of 0.002, this design allows flexibility in optimizing the antenna's operational parameters. Placing each fractal element at a distance d from the hexagonal patch's center introduces variability, not necessarily aligning with the hexagonal radiator's radius a. For a visual representation and to highlight the initial design parameter values, refer to Figure 1, showcasing the hexagon-shaped fractal antenna topology.

Each hexagon-shaped fractal antenna design parameter represents a unique design geometry feature, influencing the antenna's output characteristics individually and nonlinearly. This study focuses on enhancing the reflection coefficient ($|S_{11}|$) bandwidth, conducting a parametric analysis to pinpoint

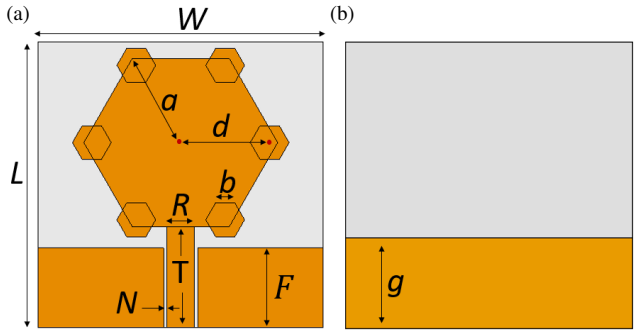

FIGURE 1. The hexagon-shaped fractal antenna with a hexagonal patch and hexagon-shaped fractal elements. $a = 8.2$ mm, $b = 1.1$ mm, $d = 7.36$ mm, $R = 2.4$ mm, $N = 0.73$ mm, $T = 8.85$ mm, $F = 7$ mm, $W = 25$, $L = 25$ mm, $g = 7.98$ mm. (a) Top view, and (b) bottom view.

features affecting this response. In this section, we discuss the impact of a, b, d, and N on $|S_{11}|$. As depicted in Figure 2(a), an increase in a value correlates with expanded upper frequencies, resulting in a bandwidth increase. Conversely, variations in b and d exhibit a decrease in upper frequencies, generating closely spaced resonating frequencies in the mid-range, illustrated in Figures 2(b)–2(c). Finally, the design parameter N, shown in Figure 2(d), exhibits minimal impact on higher and lower frequencies but significantly influences mid-range frequencies, thereby facilitating bandwidth enhancement. To understand the impact of N on the spike present around 6 GHz in our FEKO results, a simulation was carried out using another commercially available EM solver, CST Studio Suite. A comparison of the $|S_{11}|$ results for $N = 0.3$ mm in FEKO and CST is depicted in Figure 2(e). A spike can be seen clearly from the CST result around 6 GHz, validating the FEKO result. The authors believe that this is physical to the structure, i.e., inherent to the spacing or gap between the CPWs and the feedline. One possible explanation is the increase in capacitance value between the feedline and CPW as the value of N decreased from 0.7 to 0.3 mm, creating a non-resonance behavior. In summary, as the gap between the CPW and feedline decreases, a spike can be expected in any CPW-based antenna design, leading to decreased impedance bandwidth. It is ideal to retain the highest value of N possible to obtain lower values of $|S_{11}|$ and a UWB behavior.

After identifying these features, each of the selected features (i.e., a, b, d, N) was varied within the range of sample space $\{DP\}$ (units in mm): $a \in [7.8, 8.2]$, $b \in [1.1, 1.8]$, $d \in [7.2, 7.8]$, $N \in [0.3, 0.8]$ to generate the training data; that is $\{(DP^n; S_{11}^n); n = \text{number of samples in training data}\}$ these ranges were chosen purposefully to accommodate the copper patch on substrate adequately. By doing so, the goal was to encompass essential variations crucial for studying the antenna's performance without exceeding the necessary scope.

3. METHODOLOGY

3.1. Optimization Using Conventional Approach

In the quest for optimizing the hexagon-shaped fractal antenna design, a genetic algorithm (GA) within FEKO was em-

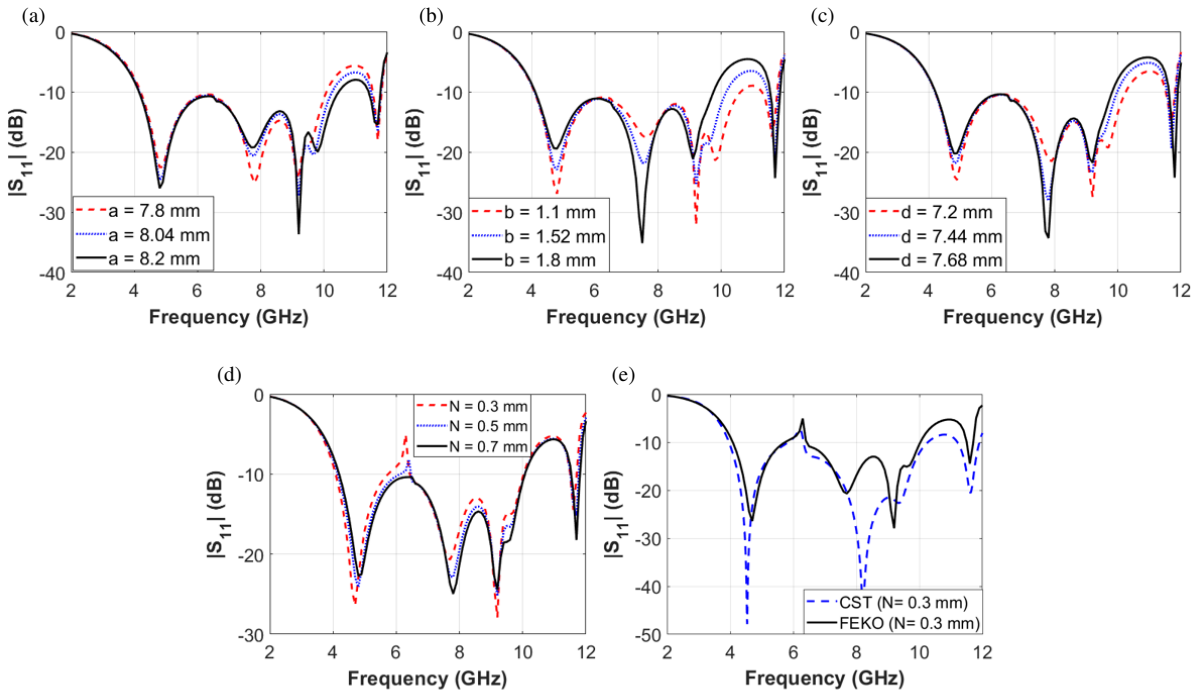

FIGURE 2. Parametric analysis of (a) hexagonal radiator a, (b) fractal element radius b, (c) distance from centers of the hexagonal radiator and fractal element d, (d) gap N, and (e) gap N (validation using CST for $N = 0.3$ mm).

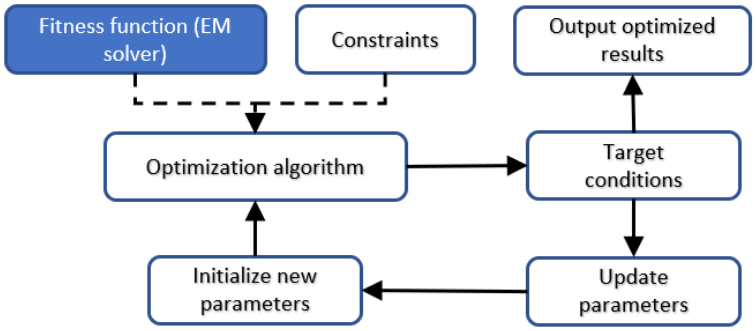

FIGURE 3. Work flow of conventional optimization with EM solver as the fitness function.

ployed. The primary objective of the GA was to minimize $|S_{11}|$ over the desired frequency range of 2 to 12 GHz while adhering to sample space $\{DP\}$. Utilizing optimization algorithms for a complicated antenna design on a local computer (Intel Core i7-10810U CPU @ 1.10 GHz) requires considerable computational resources. To examine and analyze the optimization algorithms, the Lewis HPC cluster[1] (Intel(R) Xeon(R) CPU E5-2680 v4 @ 2.40 GHz) was employed. Figure 3 depicts the workflow of a conventional optimization algorithm. The flowchart shows that the optimization algorithm repeatedly calls the fitness function (EM solver) until the target condition is met. This process can be resource-intensive as optimization algorithms must wait for EM solvers' response in each iteration.

[1]The computation for this work was performed on the high-performance computing infrastructure provided by Research Computing Support Services and in part by the National Science Foundation under grant number CNS-1429294 at the University of Missouri, Columbia, MO.

3.2. Optimization Using Machine Learning

The ML algorithms enable users to predict the output without explicit instruction. The adaptive nature of these models allows users to construct or mimic any complex system without empirical knowledge. The choice of ML models, namely radial basis function (RBF) [27, 28] and least square regression (LSR) [29], is driven by their superior generalization compared to other models available on HyperStudy. Unlike conventional optimization, a new approach to employing ML algorithms is proposed for faster and more efficient antenna output response prediction. An ML model with good generalization can mimic the EM solvers and instantly output the response. So, the conventional EM solver is replaced with a trained ML model as the fitness function in Figure 3.

3.2.1. Radial Basis Function

The output response of an antenna is a nonlinear function of input design parameters. Thus, the RBF is suitable as it converts such nonlinear input space to higher dimensional linear space to estimate the output response. The trained RBF network comprises input and output layers with only one hidden layer, and it has a specification type set as CS21 in Altair HyperStudy. Finally, to extend its utility to linear data sets, the RBF model is enhanced with a polynomial function, as depicted in Equation (2).

$$f(x) = \sum_{i=1}^{n} \lambda_i \cdot \phi\left(||x - x_i||\right) + \sum_{i=j}^{n} c_j P_j(x) \tag{2}$$

where n is the number of sampling points; x is a input vector; x_i is the i^{th} sampling point; λ_i is the coefficient of i^{th} basis function; ϕ is a basis function; $P_j(x)$ is the polynomial function; c_j is a coefficient.

3.2.2. Least Squared Regression

An LSR model (or) linear regression model is used for nonlinear data using a polynomial regression model. As the antenna output response (i.e., reflection coefficient) is a nonlinear function of input design parameters, we use a polynomial regression model of degree 1, also available in Altair HyperStudy. The LSR model is mathematically expressed in Equation (3).

$$f(x) = a_o + a_1 x_1 + a_2 x_2 + \varepsilon \tag{3}$$

where the goal of this model is to minimize the error ε between output response values of the regression model (3) and corresponding simulation model[2]. The error term is shown in Equation (3).

$$\varepsilon = \sum_{i=1}^{n} \left(f_i^{\text{predicted}} - f_i\right)^2 \tag{4}$$

3.2.3. Altair HyperStudy

The main role of Altair HyperStudy was to conduct surrogate-based optimizations utilizing trained ML models. This software enables users to import CAD designs, specifically FEKO antenna designs, without additional packages or scripting. With its intuitive interface, users can effortlessly select training data parameters, generate the necessary training data, train and validate ML models, and optimize antenna designs. Moreover, Altair HyperStudy offers the flexibility to modify optimization models' fitness functions, empowering users to tailor the process to their needs. This crucial capability facilitated the substitution of FEKO, the EM solver, with a trained ML model, enabling the seamless execution of the proposed methodology. Altair HyperStudy was employed for ML-driven antenna design optimization, leveraging its capability for surrogate-based optimizations with trained ML models. Here is a high-level breakdown of the steps followed in the approach to Altair HyperStudy:

[2]Feko, Altair Engineering, Inc.

1. Importing and Defining Parameters: The process was initiated by importing the FEKO CAD design of the hexagon-shaped fractal antenna model into Altair HyperStudy. Here, the authors defined and selected the design parameters for optimization and specified their respective ranges.

2. Model Validation and Output Definition: The imported model was validated by executing the run definition, ensuring functionality across write, execute, and extract tasks. Subsequently, the output response was defined by selecting the appropriate keyword and corresponding value from the output file. In this case, the designated keyword was $|S_{11}|$, representing the mean of $|S_{11}|$ response values obtained from 30 discrete frequency points spanning 2 to 12 GHz.

3. Data Generation with design of experiment (DOE): Training and test data were systematically generated by employing a modified extensible lattice sequence (MELS) DOE approach. MELS enabled the authors to distribute training input points evenly, thereby enhancing the model's ability to discern underlying patterns despite minimal training data.

4. Model Training and Evaluation: Utilizing the fit approach, concurrent RBF and LSR models were trained with the data generated in the previous step. The performance of these models was evaluated using root mean squared error (RMSE), refining the training process iteratively to achieve lower RMSE values while optimizing computational efficiency.

5. Integration of Genetic Algorithm Optimization: The GA optimizer was integrated into the study, designating the trained ML model as a fitness function. Alongside specifying design parameters and their ranges, constraints were incorporated to minimize the mean of the $|S_{11}|$ response. This step aimed to achieve the optimal design parameter values for the antenna.

Both of these ML models (RBF & LSR) require training data (i.e., input and output) for training the model, which are antenna design parameters and simulated output such as the $|S_{11}|$ or gain. In this study, hexagonal radiator radius 'a', fractal element radius 'b', distance from the centers of the hexagonal radiator and fractal element 'd', and the gap between ground planes on top of the substrate and the transmission line 'N' are selected to be used in the input of the training data as they have a significant impact on the $|S_{11}|$ as discussed below. $|S_{11}|$ response for each training input is used as the training data output. So, training data consists of an input matrix, '$n \times 4$', while the output matrix contains '$n \times 30$', where 'n' is the number of samples in the training data or the size of the training data set. The mean of $|S_{11}|$ responses at 30 different discrete frequency points over 2 to 12 GHz is considered for the output data. The total procedure is carried out in Altair HyperStudy [25], which enables the study and optimization of the antenna design using built-in ML algorithms. For complex antenna design, parametric analysis and optimization for a larger number of parameters is a tough job. ML models are very helpful in this scenario. With very small training data, ML models are very accurate and used as a

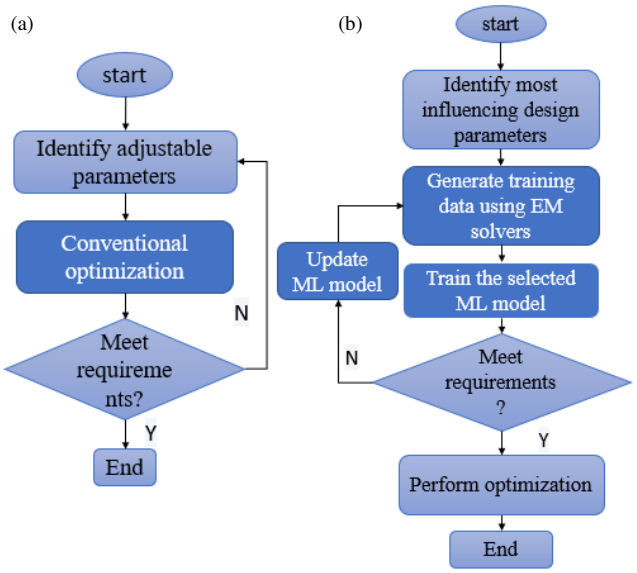

FIGURE 4. (a) Conventional optimization approach. (b) Machine learning approach.

catalyst in the optimization process. The flowchart in Figure 4 demonstrates the workflow for implementing ML models.

$$\text{RMSE} = \sqrt{\frac{1}{n}\sum_{i=1}^{n}\left(f_i^{\text{predicted}} - f_i\right)^2} \tag{5}$$

In the case of ML prediction in antenna design, finding the correct balance between the training data set size and the time required to generate is necessary. The RMSE serves as a crucial metric for assessing the variance between predicted and observed data. This study used it to measure the disparity between predicted and actual values of $|S_{11}|$. Defined mathematically by Equation (5), a good RMSE's significance hinges upon the data set's characteristics under consideration. Consequently, in determining the ideal training data size, the study opts for a size capable of yielding a lower RMSE (closer to 0) while minimizing the data generation time. From Figure 5(a), the RMSE, time values have increased with training data set size for RBF. For LSR, as depicted in Figure 5(b), the RMSE value has decreased with an increase in training data size from 5 to 15 and increased further. Training data set size 10 has less RMSE and training data generation time and is used further.

4. RESULTS AND DISCUSSION

The conventional approach (i.e., FEKO+GA) has reported the optimum design values as $a = 7.8$, $b = 1.1$, $d = 7.4$, $N = 0.3$, after 1000 (stop criteria) iterative comparisons of $|S_{11}|$ solution from fitness function (FEKO), while the ML approach optimization (i.e., RBF+GA, LSR+GA) took 1908 iterative comparisons to report design values: $a = 8.1$, $b = 1.1$, $d = 7.2$, $N = 0.6$ and $a = 8.2$, $b = 1.1$, $d = 7.2$, $N = 0.3$, respectively. The trade-off between the conventional approach and the machine learning approach is the computational time required to evaluate the fitness function in each iteration. The EM solver

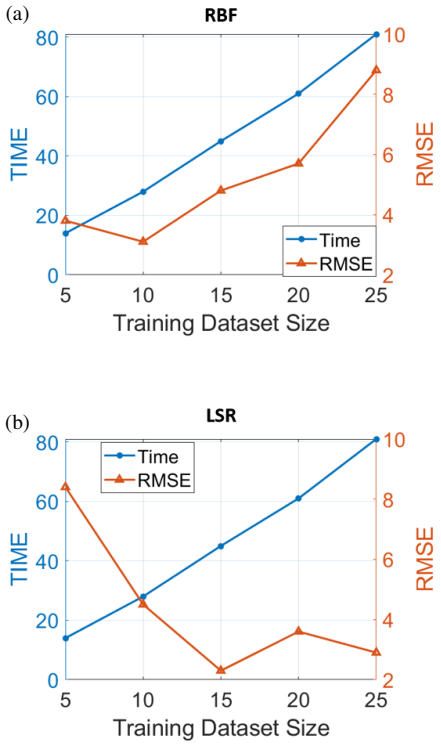

FIGURE 5. Illustration of change in ML performance metrics with training data set size for (a) RBF, and (b) LSR.

as a fitness function in conventional approach took 48 hrs on a Lewis HPC cluster[2] to obtain the above values, whereas the ML models achieved convergence to the optimization solution in just a single second on a Dell laptop with an i7 processor with 16 GB RAM to converge to the optimization solution. A comparative analysis of these approaches is presented in Table 1.

Three antennas were designed using the optimized design values obtained from FEKO+GA, RBF+GA, and LSR+GA and simulated using FEKO within the frequency range of operation and depicted in Figure 6. The sudden spike around 6.4 GHz is a simulation artifact only observed in the select cases (LSR+GA and FEKO+GA) and is probably due to the unique combination of design variables, mesh size, and the number of frequency points. The same spike is absent in the measurement

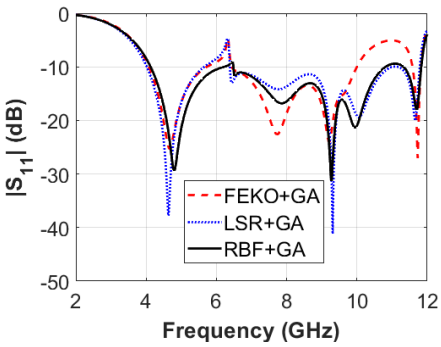

FIGURE 6. Comparision of $|S_{11}|$ response from hexagon-shaped fractal antenna designs produced from FEKO+GA, RBF+GA, and LSR+GA methods.

TABLE 1. Characteristic comparison of FEKO+GA, RBF+GA, and LSR+GA.

	RBF+GA	LSR+GA	FEKO+GA
Yielded values (mm)	$a = 8.1, b = 1.1,$ $d = 7.2, N = 0.6$	$a = 8.2, b = 1.1,$ $d = 7.2, N = 0.3$	$a = 7.8, b = 1.1,$ $d = 7.4, N = 0.3$
Computational time	$\leq$ 1 sec	$\leq$ 1 sec	48 hrs
No. of design comparisons	1908	1908	1000
% BW (simulated)	93%	98%	84%
% BW (measured)	99%	101%	76%
Training data size	10	10	NA
Computer specifications	Dell latitude 5510	Dell latitude 5510	Lewis HPC cluster[1]

TABLE 2. Comparison performance metrics of proposed method with other research works.

ML model	Training data size	No. of parameters	Optimization method	R^2	Objective
RBF (Proposed)	10	4	GA	0.9	mean ($\|S_{11}\|$)
ANN, Lasso and kNN [23]	450	5	Manual grid search	> 0.85	FOM
Modified KNN [30]	15, 8	3	Bayesian	N/A	min ($\|S_{11}\|$)

results, shown in the future sections, indicating that the spike is a simulation artifact and not a band-stop behavior. It is evident from $|S_{11}|$ solutions in Figure 6 that both the ML approaches have achieved a higher bandwidth than the conventional approach. The optimal selection of the number of training data samples hinges upon the ranges of design parameters. In our study, the parameters (a, b, d, N) were varied within a narrow range of values. Therefore, having a large training data set would result in closely spaced input values, potentially leading to redundant data during training. Choosing unique and independent values for design parameters that significantly impact the training output is crucial. This approach enables ML models to effectively discern the underlying patterns between input and output values. Table 2 presents a comprehensive comparison of various performance metrics, encompassing training data size, number of design parameters, optimization method, R^2 error, and the objective of the proposed method, against other research works. Particularly noteworthy is the achievement of a $0.9R^2$ error value with a smaller training data set in this study's RBF, underscoring a robust comprehension of the relationship between inputs and outputs.

4.1. Fabrication Results

The optimized design values obtained from the aforementioned approaches were employed in fabricating all three antennas. Due to the intricacies of the antenna design, a photolithographic method was chosen for fabrication. A 1.6 mm thick positive photoresist-laminated FR4 board was utilized, and albeit 1.5 mm thickness was desired, it was unavailable. An SMA connector was soldered to the edge of the transmission line, as depicted in Figure 7. Subsequently, a Field Fox Vector Network Analyzer was employed to measure the $|S_{11}|$ responses of all three fabricated antennas.

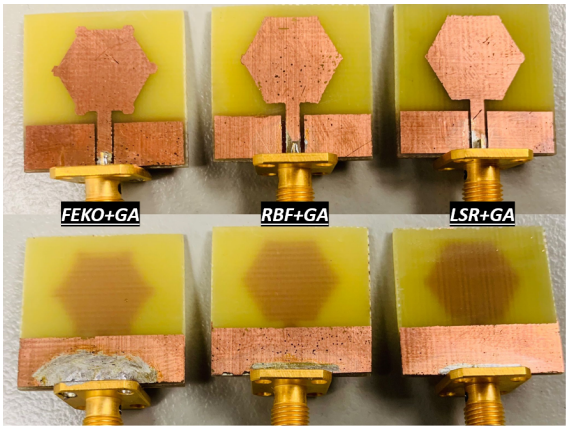

FIGURE 7. Top and bottom view of fabricated antenna designs using photolithography.

The comparison between the measured and simulated $|S_{11}|$ results is presented across three distinct scenarios. In Figure 8(a), the results for the FEKO+GA case are depicted, while Figure 8(b) showcases the outcomes for the LSR+GA scenario. Furthermore, Figure 8(c) provides the results for the RBF+GA case. There is a general agreement in all of the three cases between the measured and simulated results, particularly in terms of bandwidth, upper (F_u) and lower (F_l) cutoff frequencies. The inconsistent $|S_{11}|$ magnitude values observed in the measurements compared to the simulation values can be attributed to the multi-step fabrication process. The photolithography process was employed to fabricate the antennas due to the small size ($25 \times 25\,\text{mm}^2$) of the proposed antennas and the unavail-

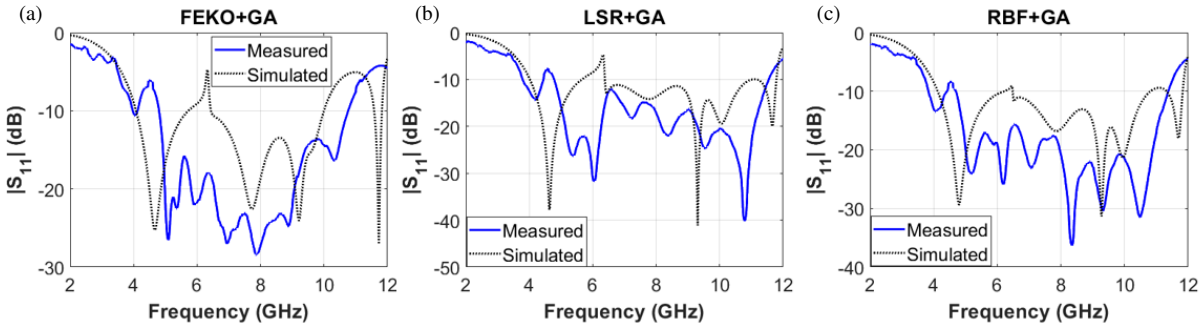

FIGURE 8. Comparison of simulated and measured $|S_{11}|$ results of (a) FEKO+GA, (b) LSR+GA, and (c) RBF+GA.

TABLE 3. Comparison of bandwidth achieved through different optimization approaches: Simulation and measurement results.

Approach	F_l (GHz)	F_u (GHz)	Percent Bandwidth (%)	Bandwidth (GHz)
Simulation (FEKO+GA)	4.07	9.99	84	5.92
Measured (FEKO+GA)	3.98	4.12	3.46	0.14
	4.80	10.76	76.61	5.96
Simulation (LSR+GA)	4.02	11.78	98	7.76
Measured (LSR+GA)	3.79	4.44	15.80	0.65
	4.79	11.54	82.67	6.75
Simulation (RBF+GA)	4.13	11.37	93	7.23
Measured (RBF+GA)	3.84	4.41	13.82	0.57
	4.70	11.37	83.01	6.67

ability of appropriate CNC drill bits in-house to create the fractals. Photolithography is a multi-step fabrication process that requires careful implementation of coating, exposure, development, and etching procedures. During the etching process, the unwanted photoresistive layer was removed using Ferric Chloride acid, making this part of the procedure challenging as some parts of the copper were accidentally removed. This resulted in uneven surface polishing and air slots on the hexagon-shaped patch antenna prototypes, notably in the LSR+GA prototype. All the above factors contributed to the slight mismatch in $|S_{11}|$ values. However, the measurements' bandwidth, F_l, and F_u values remained close to the simulated outputs and demonstrated improved bandwidth from the LSR+GA and RBF+GA cases over the FEKO+GA case.

After analyzing Table 3, it is evident that the LSR+GA optimization approach demonstrates robust performance across both simulation and photolithography methods. In particular, the photolithographic implementation of LSR+GA yields a total bandwidth of 7.4 GHz, which is 0.16 GHz higher than that of RBF+GA. Additionally, LSR+GA achieves a total percentage bandwidth of 98.47%, surpassing RBF+GA approach by a margin of 1.64%. Conversely, the FEKO+GA optimization approach exhibits comparatively limited performance, with a bandwidth of 5.92 GHz in simulation and 6 GHz in photolithography. These values are notably lower than those achieved by LSR+GA and RBF+GA methods. RBF+GA, while offering competitive performance, falls slightly behind LSR+GA in both bandwidth and percentage bandwidth. Specifically, it achieves a bandwidth of 7.24 GHz in photolithography, trailing LSR+GA by 0.16 GHz. Thus, based on these numerical comparisons, the LSR+GA optimization approach emerges as the most effective in maximizing bandwidth and percentage bandwidth, followed closely by RBF+GA, while FEKO+GA lags behind in performance metrics. The ML approach (LSR+GA) achieves a 21.3% increase in bandwidth compared to the FEKO+GA approach, validating both simulated and measured data. These findings underscore the efficacy of ML models in enhancing bandwidth. Additionally, employing ML has enabled a remarkable bandwidth enhancement while reducing computational time by over 1000 times.

$$\text{Percent Bandwidth (\%)} = \left(\frac{F_u - F_l}{F_u + F_l}\right) \times 200 \qquad (6)$$

Finally, the mathematical equation used to calculate the percentage bandwidth is provided in Equation (6), where F_u represents the upper frequency, and F_l represents the lower frequency.

The authors utilized the CST Studio Suite's frequency domain solver in combination with the GA to optimize the hexagon-shaped fractal antenna. This step aimed to compare optimization outcomes across various EM solvers (i.e., CST Studio Suite vs. FEKO). As shown in Figure 9, the optimization process achieved an 81.02% bandwidth and necessitated 24 hours of computation on the specified hardware configuration: CPU: 2xAMD EPYC 7H12 (128 cores total per node), RAM:

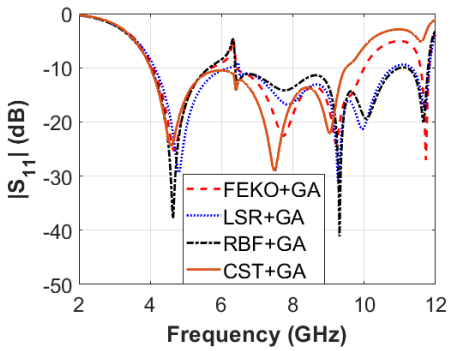

FIGURE 9. Comparison of $|S_{11}|$ response for the antenna designs produced from FEKO+GA, LSR+GA, RBF+GA, and CST+GA.

512 GB, GPU: 8xNvidia RTX A6000 with 48 GB of RAM each. In summary, the CST+GA and FEKO+GA approaches yielded the lowest percent bandwidth, albeit with longer computation times than the RBF+GA and LSR+GA approaches. The latter achieved the highest percent bandwidth within a shorter duration than the traditional optimization method.

5. CONCLUSION

In conclusion, this study presents a new methodology for optimizing UWB patch antennas by using ML algorithms, specifically RBF and LSR models. By leveraging ML models as fitness functions, this study achieves a remarkable reduction in computational time by over 1000 times while significantly enhancing antenna bandwidth by over 21.3%.

The results demonstrate the superiority of the ML-based optimization approach in both computational efficiency and antenna performance. The trained ML models accurately predict antenna responses, enabling rapid design space exploration. Fabricated antennas based on the optimized designs exhibit good agreement between simulated and measured results in terms of bandwidth and upper and lower cutoff frequencies, validating the efficacy of the ML-assisted optimization methodology. This research marks a paradigm shift in antenna design optimization, offering a transformative approach that combines advanced ML techniques with traditional optimization methods. The dramatic reduction in computational time and significant enhancement in antenna bandwidth showcase the potential of ML-based approaches to revolutionize the development of high-performance antennas for various applications.

ACKNOWLEDGEMENT

This work was funded by the U.S. Office of Naval Research (ONR) under Grant No. N00014-17-1-3016 and Grant No. N00014-22-1-2385. The authors thank Roy Allen and Peter Bland for helping with antenna fabrication and testing.

REFERENCES

[1] Mohd Isa, F. N., N. H. Kamaludin, N. F. A. Malek, and S. Y. Mohamad, "Compact UWB slotted pentagonal patch antenna for radar and communication," in *2019 IEEE International Symposium on Antennas and Propagation and USNC-URSI Radio Science Meeting*, 1393–1394, 2019.

[2] Prasad, P., S. Singh, and A. Kumar, "A wheel shaped compact UWB antenna for GPR applications," in *2021 6th International Conference for Convergence in Technology (I2CT)*, 1–5, 2021.

[3] Qi, F., F. Liang, M. Liu, H. Lv, P. Wang, H. Xue, and J. Wang, "Position-information-indexed classifier for improved through-wall detection and classification of human activities using UWB bio-radar," *IEEE Antennas and Wireless Propagation Letters*, Vol. 18, No. 3, 437–441, 2019.

[4] Cicchetti, R., E. Miozzi, and O. Testa, "Wideband and UWB antennas for wireless applications: A comprehensive review," *International Journal of Antennas and Propagation*, Vol. 2017, Article ID 2390808, 2017.

[5] Shao, W., A. Edalati, T. R. McCollough, and W. J. McCollough, "A time-domain measurement system for UWB microwave imaging," *IEEE Transactions on Microwave Theory and Techniques*, Vol. 66, No. 5, 2265–2275, 2018.

[6] Sun, J. X., Y. J. Cheng, Y. F. Wu, and Y. Fan, "Ultrawideband, low-profile, and low-RCS conformal phased array with capacitance-integrated balun and multifunctional meta-surface," *IEEE Transactions on Antennas and Propagation*, Vol. 70, No. 9, 7448–7457, 2022.

[7] John, M. and M. J. Ammann, "Antenna optimization with a computationally efficient multiobjective evolutionary algorithm," *IEEE Transactions on Antennas and Propagation*, Vol. 57, No. 1, 260–263, 2009.

[8] Recioui, A., "Concentric ring arrays optimization using the spiral inspired technique," *Algerian Journal of Signals and Systems*, Vol. 3, No. 1, 10–21, 2018.

[9] Rahmat-Samii, Y., "Genetic algorithm (GA) and particle swarm optimization (PSO) in engineering electromagnetics," in *17th International Conference on Applied Electromagnetics and Communications, 2003. ICECom 2003*, 1–5, 2003.

[10] Recioui, A., "Application of the spiral optimization technique to antenna array design," in *Handbook of Research on Emergent Applications of Optimization Algorithms*, 364–385, IGI Global, 2018.

[11] Lin, C., F.-S. Zhang, K. Dong, and Y.-C. Jiao, "Design of a modified monopole antenna using PSO based on FEKO for wireless communications," in *2010 International Conference on Microwave and Millimeter Wave Technology*, 1070–1073, 2010.

[12] Recioui, A., "Application of a hybrid Taguchi-genetic algorithm to the multiobjective design optimization of Yagi-Uda antennas," *Wireless Personal Communications*, Vol. 71, 1403–1420, 2013.

[13] Krishnan, A., A. Almadan, and A. Rattani, "Understanding fairness of gender classification algorithms across gender-race groups," in *2020 19th IEEE International Conference on Machine Learning and Applications (ICMLA)*, 1028–1035, 2020.

[14] Lo, C. Y., C.-W. Sham, and L. Ma, "A novel iris verification framework using machine learning algorithm on embedded systems," in *2020 IEEE 9th Global Conference on Consumer Electronics (GCCE)*, 173–175, 2020.

[15] Villa, M., M. Gofman, S. Mitra, A. Almadan, A. Krishnan, and A. Rattani, "A survey of biometric and machine learning methods for tracking students' attention and engagement," in *2020 19th IEEE International Conference on Machine Learning and Applications (ICMLA)*, 948–955, 2020.

[16] Degadwala, S., D. Vyas, and H. Dave, "Classification of COVID-19 cases using fine-tune convolution neural network (FT-CNN)," in *2021 International Conference on Artificial Intelligence and Smart Systems (ICAIS)*, 609–613, 2021.

[17] Sengar, P. P., M. J. Gaikwad, and A. S. Nagdive, "Comparative study of machine learning algorithms for breast cancer predic-

tion," in *2020 Third International Conference on Smart Systems and Inventive Technology (ICSSIT)*, 796–801, 2020.

[18] Günaydin, O., M. Günay, and O. Şengel, "Comparison of lung cancer detection algorithms," in *2019 Scientific Meeting on Electrical-Electronics & Biomedical Engineering and Computer Science (EBBT)*, 1–4, 2019.

[19] Vats, P. and K. Samdani, "Study on machine learning techniques in financial markets," in *2019 IEEE International Conference on System, Computation, Automation and Networking (ICSCAN)*, 1–5, 2019.

[20] Trivedi, D., A. Bhagchandani, R. Ganatra, and M. Mehta, "Machine learning in finance," in *2018 IEEE Punecon*, 1–4, 2018.

[21] Indharapu, S. S., A. N. Caruso, and K. C. Durbhakula, "Supervised machine learning model for accurate output prediction of various antenna designs," in *2022 IEEE International Symposium on Antennas and Propagation and USNC-URSI Radio Science Meeting (AP-S/URSI)*, 495–496, 2022.

[22] Wu, Q., Y. Cao, H. Wang, and W. Hong, "Machine-learning-assisted optimization and its application to antenna designs: Opportunities and challenges," *China Communications*, Vol. 17, No. 4, 152–164, 2020.

[23] Sharma, Y., H. H. Zhang, and H. Xin, "Machine learning techniques for optimizing design of double T-shaped monopole antenna," *IEEE Transactions on Antennas and Propagation*, Vol. 68, No. 7, 5658–5663, 2020.

[24] Huang, J., W. Li, Y. He, L. Zhang, and S.-W. Wong, "Optimization of antenna design using the artificial neural network and the simulated annealing algorithm," in *2021 Computing, Communications and IoT Applications (ComComAp)*, 119–122, 2021.

[25] Gampala, G. and C. J. Reddy, "Fast and intelligent antenna design optimization using machine learning," in *2020 International Applied Computational Electromagnetics Society Symposium (ACES)*, 1–2, 2020.

[26] Fallahi, H. and Z. Atlasbaf, "Study of a class of UWB CPW-fed monopole antenna with fractal elements," *IEEE Antennas and Wireless Propagation Letters*, Vol. 12, 1484–1487, 2013.

[27] Aneesh, M., J. A. Ansari, A. Singh, S. Verma, *et al.*, "RBF neural network modeling of rectangular microstrip patch antenna," in *2012 Third International Conference on Computer and Communication Technology*, 241–244, 2012.

[28] Ustun, D., M. Tekbas, and A. Toktas, "Determination of feed point by surrogate model based on radial basis function for rectangular microstrip antennas," in *2019 International Artificial Intelligence and Data Processing Symposium (IDAP)*, 1–3, 2019.

[29] Sharma, Y., J. Wu, H. Xin, and H. H. Zhang, "Sparse linear regression for optimizing design parameters of double T-shaped monopole antennas," in *2017 IEEE International Symposium on Antennas and Propagation & USNC/URSI National Radio Science Meeting*, 347–348, San Diego, CA, USA, 2017.

[30] Cui, L., Y. Zhang, R. Zhang, and Q. H. Liu, "A modified efficient KNN method for antenna optimization and design," *IEEE Transactions on Antennas and Propagation*, Vol. 68, No. 10, 6858–6866, 2020.